Transient analysis and control of a Brayton heat pump during start-up

Matteo Pettinari[a], Guido Francesco Frate[a], A. Phong Tran[b], Johannes Oehler[b], Panagiotis Stathopoulos[b], and Lorenzo Ferrari[a]

*[a] University of Pisa, Department of Energy, Systems, Territory and Construction Engineering, Pisa, Italy, matteo.pettinari@phd.unipi.it, guido.frate@unipi.it, lorenzo.ferrari@unipi.it (**CA**)*
[b] German Aerospace Center (DLR), Institute of Low-Carbon Industrial Processes, Cottbus, Brandenburg, Germany, Anh.Tran@dlr.de, Johannes.Oehler@dlr.de, Panagiotis.Stathopoulos@dlr.de

Abstract:

High-temperature heat pumps represent a valuable technology to decrease fossil fuel consumption in industry, as they can use renewable electricity to cover a given heat demand. Conventional heat pumps provide heat at temperatures around a maximum of 80 °C. Nowadays, heat production up to 150 °C can be achieved with high-temperature heat pumps. For higher temperatures between 150 °C and 250 °C, specialized designs, such as Brayton heat pumps, are required. This paper aims to investigate the transient response of the DLR's CoBra prototype, an innovative Brayton-cycle heat pump intended to provide heat above 250 °C and currently under commissioning at the DLR facility in Cottbus, Germany. First, a comprehensive transient thermodynamic model of the system is developed, accounting for heat exchangers and piping thermal inertia. Furthermore, a control logic is presented that ensures safe operation throughout off-design conditions and start-up manoeuvres. In particular, several control parameters are considered to avoid potential operational issues, such as critical temperature gradients, compressor surge, and critical mechanical vibration phenomena due to resonance. The performed simulations aim to reduce start-up time and energy consumed during start-up. Results show that with the help of the described controller, the system can reach design operation via a transient trajectory safely and quickly. Therefore, the capability of the CoBra prototype to flexibly supply high-temperature heat is demonstrated.

Keywords:

High-Temperature Heat Pump; Process Heat; Reverse Brayton Cycle; Transient Modelling; Closed Cycle Control.

1. Introduction

Heat provision accounts for over 50 % of the final energy consumption, with about 25 % for domestic purposes and space heating and 25 % for industrial processes [1]. For industrial processes, the great majority of this energy demand is met by fossil fuels. High-temperature heat pumps represent one of the most efficient options to abate emissions in this sector, as such technology may use renewable electricity to recover heat from low-temperature sources. To date, the market for industrial high-temperature heat pumps offers machines with up to 150 °C heat delivery temperature and COP values up to 5 [2–4]. Primarily fields of applications comprise the food, chemical, paper, and textile industries. Nevertheless, recent studies reported that a significant heat demand at higher temperatures currently exists in Europe [5,6], suggesting it could be addressed through heat pumps in the case higher sink heat temperatures are achieved.

Nowadays, heat pump development is limited by economic and technical barriers [2,4,7]. Economic barriers primarily consist of the long payback periods and the high ratio of electricity to gas costs. Conversely, the technical ones are related to the limited heat sink temperature and the lack of eco-compatible refrigerants performing well and safely at higher temperatures. In their investigation on the heat pumps potential for high-temperature process heat supply, Zühlsdorf et al. [3] suggest that with the proper technology, for instance, by adopting equipment already available within the oil and gas industry, sink temperatures of up to at least 280 °C can be met with heat pumps, both from a technical and economic perspective. Therefore, their scope of applications in the industry may extend.

Most heat pumps are based on the thermodynamic Rankine cycle [2]. However, other cycles can be advantageous depending on the temperature profile or the plant where they are used. In their analysis of different industrial heat consumers, Gai et al. [8] found that sometimes the transcritical, Brayton or Rankine cycle is optimal depending on the process under consideration. In particular, Brayton-based heat pumps may

https://doi.org/10.52202/069564-0076

offer more versatility in design and operability when processes characterized by large temperature glides are considered, as they use single-phase operating fluid and exchange sensible heat with the temperature sink and source [3]. Nevertheless, such systems generally offer a more straightforward construction than the Rankine or hybrid ones and also allow for partial power recovery leveraging turbo expanders. Possible processes include the food industry, with the heating of thermal oil or frying needed, hot air processes like baking or drying, paper and pulp and chemical industries but also thermal energy storage systems where Brayton heat pumps offer the advantage of supplying very high temperatures and also sub-ambient cold temperatures [9,10]. However, systems must be developed, built, and integrated into the relevant industries. Furthermore, they should be compact and provide flexibility in operation to replace or supplement current state-of-the-art gas boilers in brownfield applications. Hence, new concepts should allow for quick start-up times and load changes, ideally at high efficiencies, whilst ensuring safe operation.

To date, few Brayton-based prototypes have been proposed and developed for industrial applications [11–13], whilst most of the research focused on the energy storage field, where several projects and developers are already present on the market [14,15]. Although several research may be found in the literature discussing the cycle optimization or analysing the system behaviour in design conditions, only a few works analyse the dynamic behaviour of such plants, especially when critical operations such as start-ups are considered. In this regard, Frate et al. [16] analyzed the dynamics of a Brayron PTES during warm start-up and off-design operations. Despite not optimizing the gas turbine speed ramp for quick start-ups, a start-up time of around 30 min was reported. Smith et al. [17] presented the design of a laboratory scale pumped thermal electricity storage demonstration plant in order to test the control strategies and demonstrate the system operability and criticalities. Start-up times of around 1.38 h and 2 h were reported depending on the compressor recycle valve opening. Furthermore, Oehler et al. [12] developed and analyzed a control strategy to safely perform a cold start-up of an air-based Brayton heat pump for industrial purposes. A start-up time of more than 2.5 h and a turbine bypass valve was used to avoid compressor surge. However, the control inputs used to drive such maneuver were not designed to optimize the start-up of the system. Faster start-ups are then possible.

To further investigate in this regard, the present work analyses the transient capabilities of the Brayton heat pump proposed in [12] while undergoing a cold start-up manoeuvre. A closed-loop control system is developed and presented in the following to determine whether the system can achieve faster start-up times safely. Results aim to provide useful insights into the system's behaviour and limitations and help design an optimised procedure for quick start-ups.

2. Prototype overview

The CoBra (Cottbus Brayton Cycle) heat pump is currently under development by the German Aerospace Center (DLR) in Cottbus. Figure 1 shows the schematic and thermodynamic cycle of the heat pump.

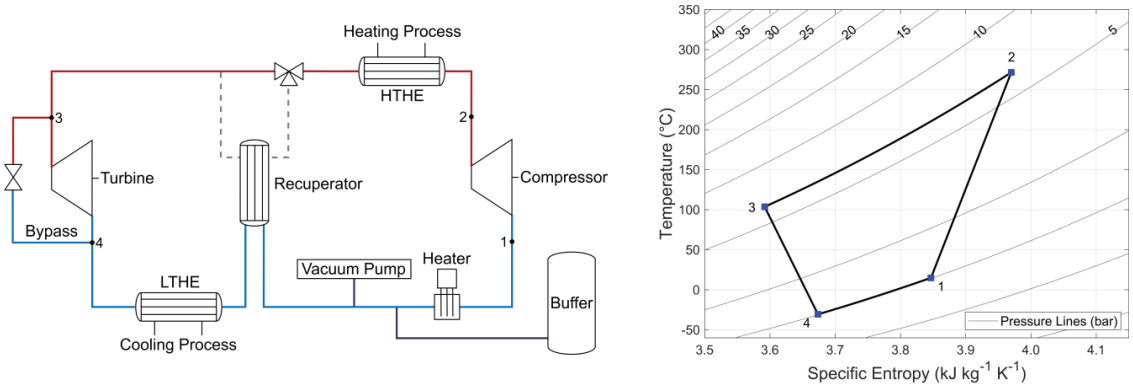

Figure. 1. CoBra heat pump: (a) system layout; (b) T-s diagram.

As a closed-loop Brayton cycle heat pump, the CoBra features a three-stage turbo compressor with pressure ratios of up to 7. The compressor raises the pressure and temperature of the working gas, which is primarily dry air but can also use other media such as argon or CO_2. With the available pressure ratios, the heat pump can achieve heat sink temperatures of 250 °C and more. After rejecting heat to a high-temperature heat sink (e.g. industrial process heat or thermal energy storage), the gas is expanded using an axial two-stage turbine, which recovers power and cools the gas to sub-ambient temperatures. A turbine bypass valve can be opened to increase the mass flow rate in the heat pump, thereby stabilizing the compressor flow. In the low-temperature heat exchanger, the gas absorbs heat from a heat source before returning to the

https://doi.org/10.52202/069564-0076

compressor. An internal recuperator may leverage the remaining temperature difference between the heat exchanger outlet flows to raise the temperature at the compressor inlet. All three heat exchangers are shell-and-tube heat exchangers. The heat pump cycle is nearly hermetically sealed, thus enabling load variation via injection or air removal. Using valves and pressurized buffer storages, the system pressures and, consequently, the load can be controlled [11].

3. Dynamic modelling methodology

A transient model of the CoBra heat pump was developed through the Simulink® environment of Matlab® R2022b [18]. In particular, the Simscape™ libraries were used as they provide built-in models for all the main components constituting the plant. As for the system fluid, dry air was considered and treated as real gas. Its thermophysical properties were retrieved through RefProp [19].

3.1 Turbomachinery

The compressor and turbine were modelled from a system level by using custom components available in Simscape™. The mathematical model of each element comprises continuity equations, such as mass and energy balances. In particular, mass is conserved such that:

$$\dot{m}_{in} + \dot{m}_{out} = 0, \tag{1}$$

where $\dot{m}_i$ are the inlet and outlet mass flow rates, respectively. In a similar fashion, energy balance is computed as:

$$\dot{\Phi}_{in} + \dot{\Phi}_{out} + \dot{W}_{fluid} = 0, \tag{2}$$

where $\dot{\Phi}_i$ are the inlet and outlet energy fow rates, and $\dot{W}_{fluid}$ is the power delivered to/done by the operating fluid (e.g., $\dot{W}_{fluid} = |\dot{W}_{fluid}|$ in case of a compressor, and $\dot{W}_{fluid} = -|\dot{W}_{fluid}|$ in case of a turbine), defined as:

$$\dot{W}_{fluid} = \dot{m}_{in} \frac{\Delta h_{is}}{\eta_{is}}, \tag{3}$$

where $\dot{m}_{in}$ is the inflow mass flow rate, Δh_{is} is the specific enthalpy isentropic variation, and η_{is} is the turbomachine isentropic efficiency. Compressor and turbine mechanical powers are respectively computed according to Eq. (4) and Eq. (5):

$$\dot{W}_c = \frac{\dot{W}_{fluid}}{\eta_m}, \tag{4}$$

$$\dot{W}_t = \eta_m \dot{W}_{fluid}, \tag{5}$$

where η_m is the turbomachine mechanical efficiency. As for the design and off-design modelling, performance maps were used, therefore establishing the relationship between the machines inlet conditions (e.g., mass flow rate, temperature, and pressure) and quantities such as pressure ratio and isentropic efficiency. Figure 2 reports the performance maps considered in this work. Corrected parameters, defined as in Eq. (6), were used to account for variations at the machine inlet:

$$\begin{cases} \dot{m}_{corr} = \dfrac{\sqrt{T_{in}/T_0}}{p_{in}/p_0} \\ n_{corr} = \dfrac{n}{\sqrt{T_{in}/T_0}} \end{cases}, \tag{6}$$

where p_0 = 101325 Pa and T_0 = 288.15 K. Furthermore, turbomachines were assumed adiabatic with neglibile volume. Their thermal dynamic was therefore neglected. Conversely, inertial effects were considered by accounting for the compressor, turbine, motor, generator, and transmission moments of inertia. Inertial torques were therefore computed as:

$$\tau = J\dot{\omega}, \tag{7}$$

where J is the moment of inertia of the component, whilst $\dot{\omega}$ is its angular acceleration. Finally, coupling between compressor and motor, as well as turbine and generator, was assumed ideal. Hence, gearboxes losses due to backlash and friction were neglected.

3.2. Heat exchangers

Similarly to the turbomachinery, the shell-and-tube heat exchangers were modelled through Simscape™ Fluids library components. Heat exchangers were assumed adiabatic with and a fixed-volume construction to capture variations in fluid mass flow rates due to compressibility. Therefore, mass is conserved along the tube/shell side of the exchanger such that:

https://doi.org/10.52202/069564-0076

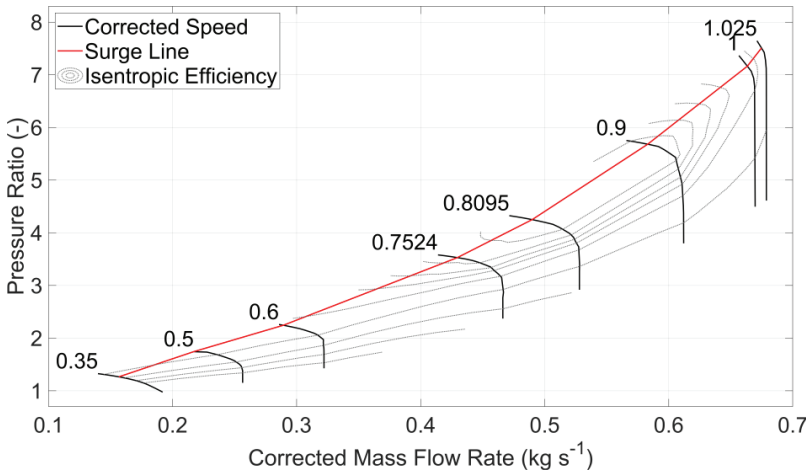

Figure. 2. Compressor map.

$$\left[\left(\left(\frac{\partial\rho}{\partial \mathrm{p}}\right)_u \frac{d\mathrm{p}_I}{dt} + \left(\frac{\partial\rho}{\partial \mathrm{u}}\right)_p \frac{d\mathrm{u}}{dt}\right]\right] \mathrm{V} = \dot{\mathrm{m}}_{\mathrm{in}} + \dot{\mathrm{m}}_{\mathrm{out}}, \tag{8}$$

where $\dot{\mathrm{m}}_{\mathrm{i}}$ are the mass flow rates at the inlet/outlet of the tube or shell side, whilst ρ, p_I, u, and V are the gas mass density, pressure, specific internal energy, and volume, respectively. Pressure losses were modelled as:

$$\Delta \mathrm{p} = \left(\frac{\rho_{\mathrm{nom}}}{\rho}\right)\left(\frac{\dot{\mathrm{m}}^2}{\dot{\mathrm{m}}_{\mathrm{nom}}{}^2}\right)\Delta \mathrm{p}_{\mathrm{nom}}, \tag{9}$$

where the subscript $_{\mathrm{nom}}$ refers to the thermophysical quantities evaluated when the system operates at nominal conditions. Furthermore, energy is conserved such that:

$$\left[\left(\left(\frac{\partial \mathrm{U}}{\partial p}\right)_{\mathrm{T,V}} \frac{d\mathrm{p_I}}{dt} + \left(\frac{\partial \mathrm{U}}{\partial \mathrm{T}}\right)_{\mathrm{p,V}} \frac{d\mathrm{T_I}}{dt}\right]\right] = \dot{\Phi}_{\mathrm{in}} + \dot{\Phi}_{\mathrm{out}} + \dot{\mathrm{Q}}, \tag{10}$$

where $\dot{\Phi}_{\mathrm{i}}$ are the energy flow rates at the tube or inlet/outlet, $\dot{\mathrm{Q}}$ is the heat transfer rate exchanged between the two fluids, and $\mathrm{p_I}$, $\mathrm{T_I}$, and U are the pressure, temperature and internal energy of the gas volume, respectively.

As for the heat transfer through the heat exchanger, it was determined according to the ε-NTU method. At each simulation step, the number of transfer units (NTU) was therefore computed as:

$$\mathrm{NTU} = \frac{1}{\mathrm{C_{min}R_{overall}}}, \tag{11}$$

where $\mathrm{C_{min}} = \min\left(\mathrm{c_{p,tube}}\dot{\mathrm{m}}_{\mathrm{tube}}; \mathrm{c_{p,shell}}\dot{\mathrm{m}}_{\mathrm{shell}}\right)$, whilst $\mathrm{R_{overall}}$ is the overall thermal resistance defined as:

$$\mathrm{R_{overall}} = \frac{1}{\alpha_{\mathrm{tube}}\mathrm{A_{tube}}} + \mathrm{R_{foul,tube}} + \mathrm{R_{wall}} + \mathrm{R_{foul,shell}} + \frac{1}{\alpha_{\mathrm{shell}}\mathrm{A_{shell}}}, \tag{12}$$

where α_{i} are the convective heat transfer coefficients of the fluids flowing within the tube/shell, $\mathrm{A_i}$ are the aggregate heat transfer surface areas, $\mathrm{R_{foul,i}}$ are the fouling resistances, and $\mathrm{R_{wall}}$ is the wall interface thermal resistance. The heat exchanger effectiveness was then computed as a function of the NTU value through correlations based on the heat exchanger type [20].

In order to capture the thermal transient due to the heat exchangers mass, the wall thermal mass was defined as:

$$\mathrm{C_{wall}} = \mathrm{c_{p,wall}}\mathrm{M_{wall}}, \tag{13}$$

where $\mathrm{c_{p,wall}}$ is the wall specific heat, and $\mathrm{M_{wall}}$ is its inertial mass. Therefore, the heat transfer rate exchanged across the heat exchanger was determined according to:

$$\dot{\mathrm{Q}}_{\mathrm{tube}} = \varepsilon\dot{\mathrm{Q}}_{\mathrm{max}} + \mathrm{C_{wall,tube}}\dot{\mathrm{T}}_{\mathrm{wall,tube}}, \tag{14}$$

$$\dot{\mathrm{Q}}_{\mathrm{shell}} = \varepsilon\dot{\mathrm{Q}}_{\mathrm{max}} - \mathrm{C_{wall,shell}}\dot{\mathrm{T}}_{\mathrm{wall,shell}}, \tag{15}$$

https://doi.org/10.52202/069564-0076

where $C_{wall,i} = \frac{C_{wall}}{2}$ is the thermal capacity evenly divided between the two sides of the heat exchanger, $\dot{T}_{wall,i}$ is the rate of change in temperature in the wall half (positive if the temperature increases, negative when it drops), and $\dot{Q}_{max}$ is the ideal heat transfer rate. Finally, to improve simulation accuracy, each heat exchanger was modelled as a series of ten components characterized by the mathematical model described above. Hence, nominal gas volumes, heat transfer surface areas, as well as pressure losses have been evenly distributed among the elements.

3.3. Piping

As piping represents a non-negligible fraction of the gas volume of the system volume, it was considered and distributed throughout the model according to the actual plant layout. Similarly to the heat exchangers, pipe components conserve energy as in Eq. (10), whilst mass is conserved such that:

$$\left[\left(\left(\frac{\partial M}{\partial p}\right)_{T,V}\frac{dp_I}{dt} + \left(\frac{\partial M}{\partial T}\right)_{p,V}\frac{dT_I}{dt}\right] = \dot{m}_{in} + \dot{m}_{out}. \tag{16}$$

Momentum balance was determined by assuming the pipe in half. Hence, the momentum flux and the viscous friction of each half were computed as:

$$p_i - p_I = \left(\frac{\dot{m}_i}{S}\right)^2\left(\frac{1}{\rho_i} - \frac{1}{\rho_I}\right) + \Delta p_{iI}, \tag{17}$$

where the subscripts $_i$ and $_I$ refer to the pipe inlet/outlet and gas volume nodes, respectively, S is the pipe cross-sectional area, and Δp_{iI} are the pressure losses due to viscous friction, computed accordingly to the flow regime. As for the heat transfer occurring throughout the pipe, it was modelled as:

$$\dot{Q} = \dot{Q}_{conv} + \dot{Q}_{cond}, \tag{18}$$

where $\dot{Q}_{conv}$ is the convective heat transfer between the pipe wall and the gas volume, whilst $\dot{Q}_{cond}$ denotes the heat transfer within the pipe material. By assuming an exponential distribution along the pipe, the convective heat transfer was computed as:

$$\dot{Q}_{conv} = \left|\dot{m}_{avg}\right| c_{p,avg}\left(1 - \exp\left(-\frac{\alpha_{avg}A}{\left|\dot{m}_{avg}\right| c_{p,avg}}\right)(T_{wall} - T_{in}) + -\frac{k_I A}{d_h}(T_{wall} - T_i)\right), \tag{19}$$

where $\dot{m}_{avg}$ is the average mass flow, $c_{p,avg}$ is the specific heat evaluated at the average gas temperature, α_{avg} is the convective coefficient computed by considering the gas thermal conductivity at average temperature (k_{avg}), A is the pipe surface area, d_h is hydraulic diameter, and T_{wall}, T_i, T_{in} are the wall, gas volume, and inlet mass flow rate temperatures, respectively. Finally, the heat transfer due to the conduction within the pipe metal was computed as:

$$\dot{Q}_{cond} = 2\pi k_{mat} L\left[\frac{(T_{mat} - T_{in})}{\ln\left(\frac{d_{avg}}{d_{in}}\right)} + \frac{(T_{out} - T_{mat})}{\ln\left(\frac{d_{out}}{d_{avg}}\right)}\right] + c_{mat} M_{mat} \dot{T}_{mat}, \tag{20}$$

where L is the pipe length, k_{mat}, c_{mat}, M_{mat}, $\dot{T}_{mat}$ are the thermal conductivity, specific heat, inertial mass, and temperature of the pipe material, d_i are the pipe inner, mean, and outer diameters, and T_i are the respective metal temperatures.

3.4. Valves and other equipment

The transient model also accounted for the ancillary equipment reported in Figure 1a. Hence, valves were modelled as adiabatic variable restrictions with negligible volume. In particular, the three-way valve was modelled through two inversely linked valves, such that opening one valve results in the closing of the other. Furthermore, valve geometry was characterized based on manufacturer data, and a linear flow characteristic was considered. As for the heater, only pressure drops were accounted for and modelled as in Eq. (9).

3.5. Controls

Two independent control loops were implemented to simulate the system in transient conditions, namely:

- anti-surge controller;
- temperature controller.

The anti-surge controller was designed to prevent the compressor from operating within critical regions in proximity to the surge line. With reference to Figure 1a, compressor surge was avoided by manipulating the turbine bypass opening, thus increasing the primary mass flow rate. The valve opening was regulated by a

https://doi.org/10.52202/069564-0076

variable-gain PI feedback controller based on the surge margin error. In the present work, the surge margin was defined as:

$$\mathrm{SM} = \left(\frac{\mathrm{PR_{surge}}}{\mathrm{PR_{op}}} - 1\right)_{\dot{m}_c}, \tag{21}$$

where $\mathrm{PR_{op}}$ is the actual pressure ratio, while $\mathrm{PR_{surge}}$ is the surge line pressure ratio evaluated at the same reduced flow. Controller gains were determined to provide a pure proportional action at high errors to ensure a prompt response in case of critical operating conditions. An integral control action was gradually added at low errors for setpoint tracking.

On the other hand, the temperature controller varies the compressor shaft speed in order to control the compressor outlet temperature. As discussed in [12], the control requirements were set as follows:

temperature slopes of no more than 2 K/min to avoid critical thermal stresses at the heat exchangers;

fast crossing of critical low speeds to avoid resonance effects of the compressor shaft.

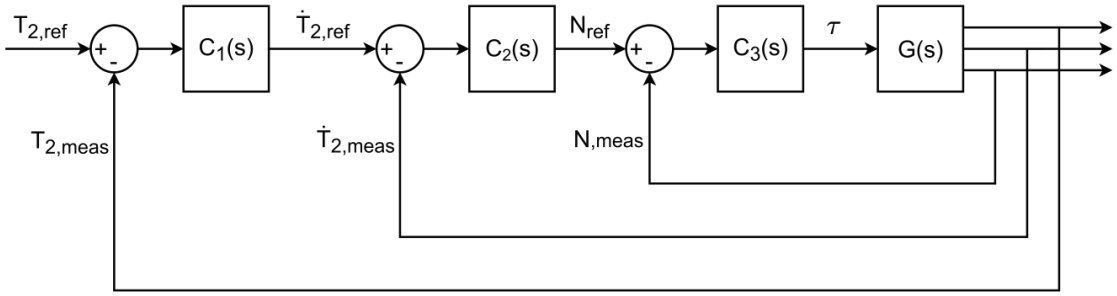

Figure. 3. Simplified temperature control schematic.

A cascade control architecture, made of three nested loops, was found suitable for the given requirements. The compressor outlet temperature was chosen as the primary controlled variable, as measuring the temperature inside the heat exchanger is a non-trivial task. As shown in Figure 3, the outer regulator uses the temperature error to determine a setpoint for the compressor outlet temperature slope. Here, the slope setpoint is limited to a maximum value of 2 K/min. Subsequently, the intermediate control loop processes the temperature slope setpoint and compares it with the actual measurement/estimation to provide a motor speed setpoint. Similar to the outer loop, the speed setpoint is limited to values within the compressor's operating range. Finally, an inner loop determines the motor torque based on the difference between the reference and measured motor speed.

It is worth mentioning that sensor and controller dynamics are negligible as they are faster than the ones characterizing the system under analysis. Nevertheless, standard anti-windup techniques were employed to manage the undesired effects related to the interaction between the controllers' integral actions and the saturations characterizing the physical system and the control schemes.

3.6. Transient simulation

The model outlined in the previous sections was used to investigate the system's transient behaviour during the start-up, aiming at determining the characteristic time and the significant criticalities that occur while performing such a manoeuvre.

At first, a cold start-up manoeuvre was simulated while imposing a maximum temperature slope of 2 K/min. The start-up time was assumed to be when the system provides heat at a temperature with an absolute error of less than one degree with respect to the design value. Secondly, a sensitivity analysis was performed by varying the maximum allowed slope in the 2−50 K/min range to investigate how the start-up time of the system is affected by the temperature slope limit.

Each simulation scenario was initialized through the same initial conditions. In particular, initial conditions were computed such that the system had enough mass to reach nominal conditions at the end of the start-up. Therefore, the initial system pressure was assumed to be almost 2 bar, whilst the initial fluid and metal temperatures were set between 15−20 °C. Mass flow rates on the secondary side of the cycle heat source and sink heat exchangers were considered constant throughout the simulation and were already at their nominal values. The turbine and generator were supposed to rotate at their respective design speeds. Conversely, the motor and compressor were assumed to rotate very slowly (~3 % of the nominal speed) to avoid numerical instability during the transient initialization of the model. Finally, control actuators such as the heater and the recuperation valve three-way were not considered during the start-up manoeuvre. In particular, the three-way valve was set such that the primary mass flow exiting the high-temperature heat

exchanger went directly to the turbine inlet. Therefore, the recuperator was disabled and a non-regenerated configuration of the plant was assumed.

4. Results and discussion

4.1. Cold start-up

During the cold start-up, the system goes from steady conditions to nominal ones based on the control inputs determined by the temperature and anti-surge regulators. Control input and outputs are reported in Figure 4.

At the beginning of the simulation, the system is at an ambient temperature at a pressure of 2 bar. As the compressor rotates at low speeds, corrected flow is negligible. The surge margin is less than 10% (e.g., minimum allowable value), and the bypass valve is fully open due to the anti-surge controller action (Figure 4a). Moreover, as the compressor outlet temperature is lower than 271 °C (e.g., the desired setpoint), the temperature controller causes the motor/compressor to accelerate (Figure 4b). Consequently, the compressor outlet temperature increases, as reported in Figure 5a, whilst the turbine inlet temperature remains constant as heat is absorbed by the high-temperature heat exchanger. Since the bypass is fully open, part of the primary mass flow does is not expanded by the turbine, and only a minor temperature drop

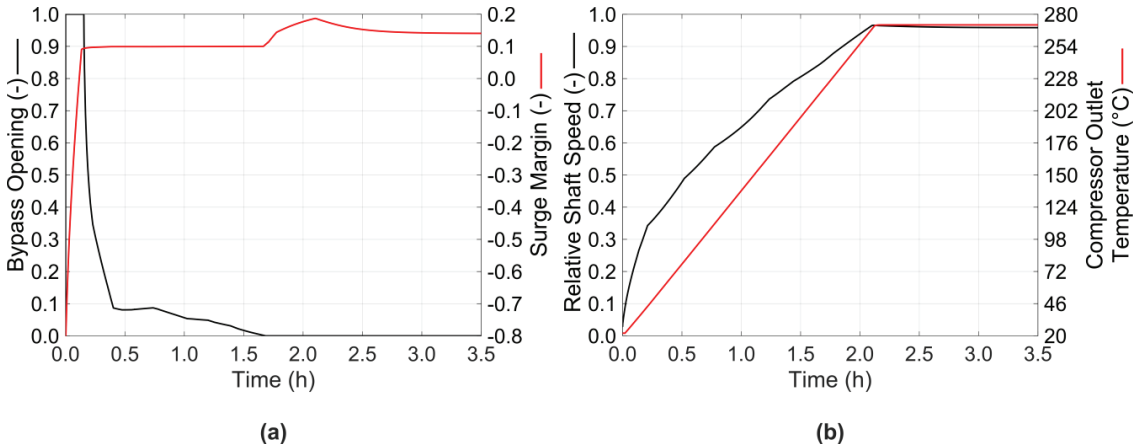

Figure. 4. Control signals (in blue) against controlled variables (orange): (a) surge margin controller ($SM_{ref} = 10\%$); (b) compressor outlet temperature controller ($T_{2,ref} = 271°C$).

occurs through the valve. The system operates in the abovementioned configuration for almost ten minutes. In such a period, the compressor keeps accelerating, increasing its outlet temperature and reducing the surge margin. As a result, the operating point slowly moves toward higher speeds and efficiencies on the right of the compressor map at an almost constant pressure ratio (Figure 6).

At t = 9 min, the surge margin becomes greater or equal to the minimum allowable limit. Since the compressor keeps accelerating, the anti-surge regulator gradually closes the bypass valve to maintain the setpoint surge margin. In more detail, the bypass valve goes from 100% open down to around 10 % open at t = 23 min, and it is fully closed after t = 1.67 h, as shown in Figure 4a. Due to the bypass closure, part of the primary mass flow expands through the turbine, and consequently, the temperature at the turbine outlet starts to decrease (Figure 5a). Also, the pressure ratio progressively increases because of the higher rotational speed (Figure 5b). As a result, the operating point moves toward higher speeds and efficiencies parallel to the surge line.

At t = 1.67 h, the anti-surge controller fully closes the bypass valve as the system operates safely away from the surge line. On the other hand, slightly after two hours, the compressor outlet temperature reaches the design value, and the temperature regulator stops accelerating the compressor. The system operates close to the design conditions at this point, providing a heat flow rate of 115 kW at around 262 °C. From here to the end of the simulation, the temperature controller provides only minor adjustments. In particular, the motor/compressor speed slightly decreases as a consequence of the stabilization of the system temperatures, which is not instantaneous due to the thermal inertia of the system (e.g., T_3, T_4 and T_{wall}). This can also be observed in Figure 6, where the compressor operating point remains almost in the same position on the map, experiencing only a minor displacement toward higher efficiencies and pressure ratios as the temperatures settle.

It is worth noting that, during the transient, the compressor outlet temperature increases at a constant slope, which is maintained below the maximum allowable value by the temperature controller. Limiting the compressor outlet temperature helps contain the temperature gradients within the heat exchangers. For

https://doi.org/10.52202/069564-0076

instance, by looking at Figure 5a, it can be observed that the metal temperature at the high-temperature heat exchanger inflow shows a similar trend after a delay of almost 12 min caused by the thermal mass of the piping and the first element of the heat exchanger. A significant delay can also be noted in the turbine inlet temperature as it increases only after 40 min with respect to the compressor outlet temperature. Here, the delay magnitude is higher as it accounts for the thermal inertia of the complete high-temperature heat exchanger and the piping connecting the heat exchanger with the expander. Furthermore, as the temperature slope is determined based on the capability of the heat exchangers to sustain thermal stresses, it can be stated that their design represents a critical constraint for quick plant start-up.

It can be further noted that the motor/compressor speed increases quickly, especially at the lower values, ensuring the compressor never operates at critical speeds for an extended amount of time, thus avoiding potential deleterious effects related to compressor shaft vibrations. Moreover, the motor/compressor acceleration is continuously modulated as a reaction to the bypass valve closure, thereby denoting interaction and the goodness of the developed control system.

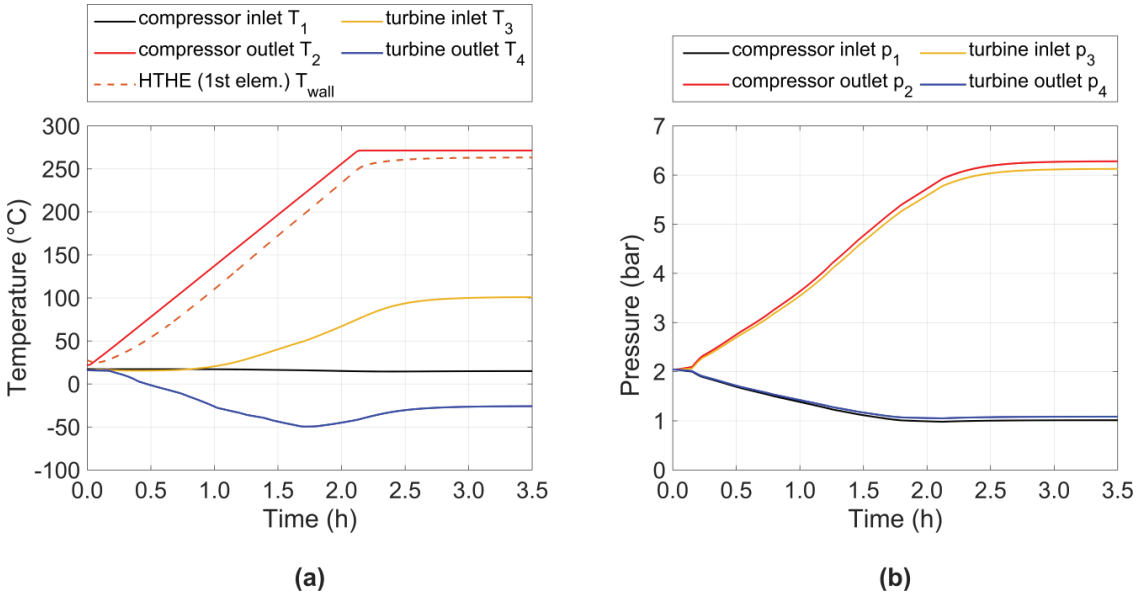

Figure. 5. System transient response during a cold start-up: (a) cycles temperatures and HTHE first element average wall temperature; (b) cycle pressures.

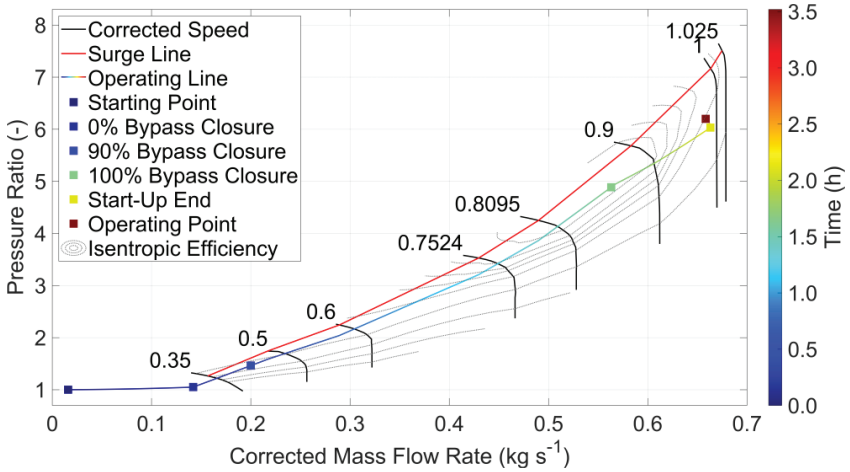

Figure. 6. Compressor operating line during the start-up.

4.2. Sensitivity analysis

The previous section showed that the thermal stresses sustainable by the heat exchangers mainly constrain the start-up time of the system. Hence, a sensitivity analysis was performed to further investigate such a relationship. The system's start-up was simulated by varying the maximum allowable slope at the compressor outlet temperature in the 5−50 K/min range with a 5 K/min step. Each simulation was initialized as discussed in Section 3.6. Results are summarized in Figure 7, which reports the start-up times and system power consumption as a function of the maximum allowable slope of the compressor outlet temperature.

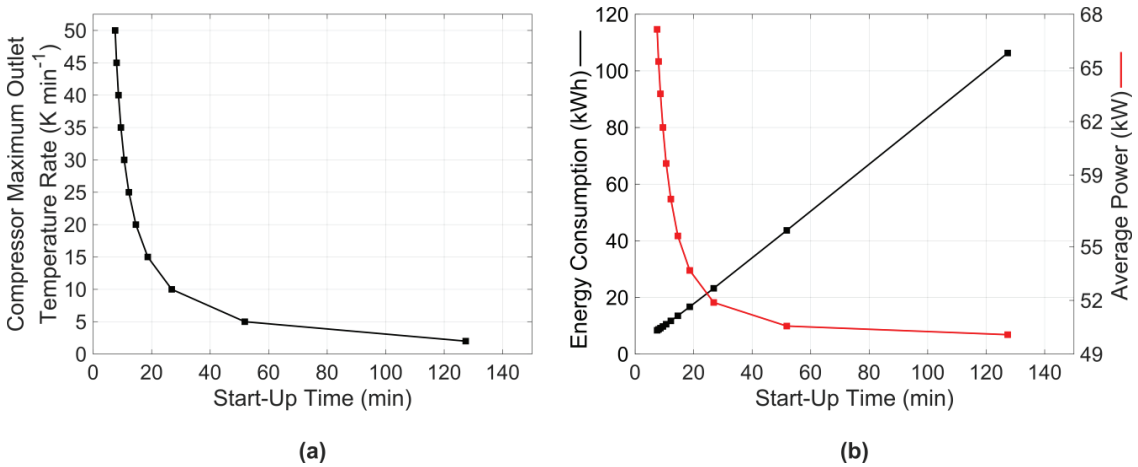

Figure. 7. Sensitivity to the maximum compressor outlet temperature rate: (a) start-up time; (b) energy consumption and average absorbed power during the start-up.

It can be observed that start-up time significantly reduces as the slope constraint is relaxed (Figure 7a). For instance, allowing for a temperature slope of 5 K/min leads to a start-up time of around 52 min (e.g., 60 % reduction), whilst in case of a slope of 10 K/min, the start-up time drops to 27 min (e.g., 80 % reduction), providing more flexibility of use in real applications. From there on, minor advantages are shown for higher temperature slopes. However, it is worth noting that such temperature slopes would require suitably designed heat exchangers, potentially increasing the capital cost of the plant and thus making it less appealing from an economic perspective. It can also be noticed that the system's energy consumption decreases almost linearly with the start-up time reduction (Figure 7b). Therefore, higher temperature slopes lead to lower energy consumption. On the other hand, less conservative slopes cause higher average power absorbed by the system increases, with a trend similar to the one reported in Figure 7a.

Apart from the considerations discussed above, shortening the start-up may lead to new technical challenges to be addressed. For instance, Figure 8 reports the cycle temperatures trend for a maximum temperature slope of 2, 10, and 15 K/min while performing the start-up.

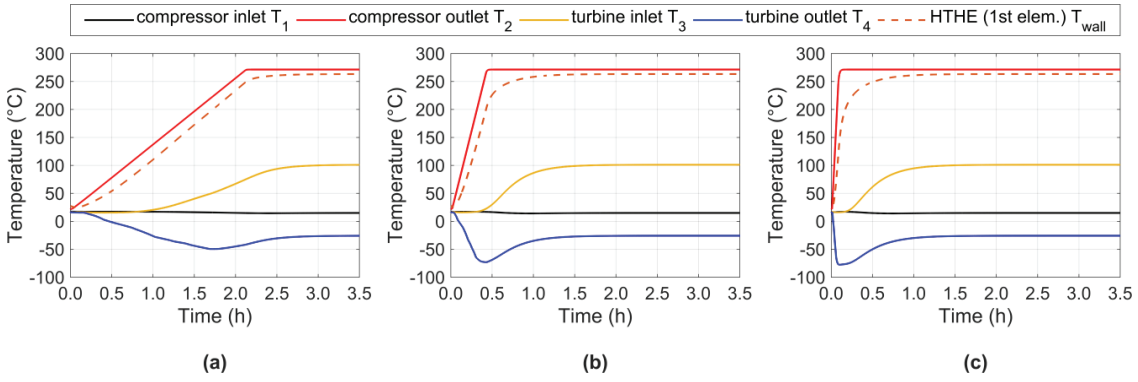

Figure. 8. Cycle and HTHE tube inlet temperatures for different values of temperature rate constraint at the compressor outlet: (a) $\dot{T}_2 = 2$ K min^{-1}; (b) $\dot{T}_2 = 10$ K min^{-1}; (c) $\dot{T}_2 = 50$ K min^{-1}.

https://doi.org/10.52202/069564-0076

It can be observed that higher allowable slopes lead to faster accelerations of the compressor, causing a quicker increase in both mass flow rate and pressure ratio. During rapid acceleration manoeuvres, the target pressure ratio and the bypass valve closing are reached before the metal temperatures in the high-temperature heat exchanger have settled. This leads to low turbine inlet temperatures and, consequently, turbine outlet temperatures of below −50 °C. As these low temperatures may lead to icing at the turbine outlet, further solutions are needed to handle these problems. A possible workaround may involve regulating the turbine shaft speed to operate with lower isentropic efficiencies, thereby mitigating the low outlet temperatures. However, at this stage of the work, it is not yet clear whether their adoption may affect the final start-up time of the plant. Therefore, further investigations must be conducted in this regard.

5. Conclusions

This paper investigates the transient behaviour of the DLR's CoBra heat pump during a cold start-up, assessing the time needed to reach design conditions and studying potential criticalities while performing such a manoeuvre. To this extent, a thermodynamic model of the system, comprehensive of mechanical, thermal and volume dynamics, was developed based on actual data characterizing the prototype. In addition, a control strategy was designed to automatically drive the compressor whilst ensuring the safe operation of the plant.

Results show the time needed to perform a cold start-up is around 2 hours when a maximum temperature slope is limited to 2 K/min to prevent thermal stresses at the heat exchangers. As expected, mechanical and pressure transient effects showed to be negligible when compared to the thermal dynamics characterizing the heat exchangers and piping. In particular, the heat exchangers showed delays of around 40 min.

Further analysis showed faster start-ups are possible in the case of less conservative temperature slopes. For instance, by increasing the maximum allowable slope to 5 or 10 K/min through adopting more advanced heat exchangers, the start-up time decreases to 52 and 27 min (e.g., start-ups shorter by more than 50 % and 80 % compared to a slope limit of 2 K/min). However, it was observed that quicker start-ups might lead to undesired effects at the turbine, as the outlet temperatures go below −70 °C during the transient, potentially causing icing. Further work is then required to assess the magnitude of these issues and to investigate whether possible solutions may negatively affect the start-up time of the plant, therefore nullifying the economic effort of using more sophisticated heat exchangers.

Finally, it is worth mentioning that the considered Brayton heat pump showed a start-up time consistent with the ones reported for a similar cycle specifically designed for energy-storage purposes [17], where start-up times in the 1.38−2 h range have been reported depending on the opening the compressor recycle valve opening. Here, differences in the results may be due to the different designs of the components, operating modes, temperature levels, and heat exchangers' size or technology, as the system are meant for different purposes. Although the comparison may suggest the validity of the proposed analysis, the proposed results should be confirmed through experimental data. Therefore, future work must be conducted in this direction in order to validate and further improve the developed transient model of the Brayton heat pump.

Acknowledgments

This research has received financial contribution from the Italian Operative National Plan (Piano Operativo Nazionale, PON) in the framework of the project Ricerca e Innovazione 2014−2020 (PON R&I) – Azioni IV.4 e IV.5 "Dottorati di ricerca su tematiche dell'innovazione e green" (DM MUR 1061/2022) e IV.6 "Contratti di ricerca su tematiche dell'innovazione e green" (DM MUR 1062/2022)

Nomenclature

Abbreviations:

CoBra	Cottbus Brayton cycle heat pump
NTU	Number of Transfer Unit
HTHE	High-Temperature Heat Exchanger
LTHE	Low-Temperature Heat Exchanger

Letter symbols:

$\dot{m}$	mass flow rate, kg/s
T	temperature, °C
p	pressure, Pa
V	volume, m^3
h	specific enthalpy, J/kg
u	specific internal energy, J/kg
U	internal energy, J

$\dot{W}$	power, W
n	rotational shaft speed, rad/s
J	moment of inertia, kg/m^2
$\dot{M}$	mass accumulation, kg/s
$\dot{Q}$	heat transfer rate, W
C	heat capacity rate, W/K
c	specific heat, J/(kg K)
R	thermal resistance, K/W
A	heat transfer surface area, m^2
S	cross-sectional area, m^2
k	thermal conductivity, W/(m K)
d	diameter, m

Greek symbols

η	efficiency
Φ	energy flow rate, W
τ	torque, N m
$\dot{\omega}$	component rotational acceleration, rad/s^2
ρ	mass density, kg/m^3
α	convective heat transfer coefficient, W/(m^2 K)
ε	effectiveness

Subscripts and superscripts

0	reference state
1,2,3,..	cycle points
i	*i*-th element
p	at constant pressure
u	at constant specific internal energy
T	at constant temperature
V	at constant volume
in	inlet/inner
out	oulet/outer
is	isentropic
$fluid$	fluid
$corr$	corrected
I	internal/gas volume
$overall$	overall
$foul$	fouling
hot	hot fluis/side
$cold$	cold fluid/side
$wall$	wall
rel	relative
h	hydraulic
$conv$	convective
$cond$	conductive
avg	average
mat	material

References

[1] IEA, 2022, *Heating*, IEA, Paris.

https://doi.org/10.52202/069564-0076

[2] Arpagaus, C., Bless, F., Uhlmann, M., Schiffmann, J., and Bertsch, S. S., 2018, “High Temperature Heat Pumps: Market Overview, State of the Art, Research Status, Refrigerants, and Application Potentials,” Energy, **152**, pp. 985–1010. https://doi.org/10.1016/j.energy.2018.03.166
[3] Zühlsdorf, B., Bühler, F., Bantle, M., and Elmegaard, B., 2019, “Analysis of Technologies and Potentials for Heat Pump-Based Process Heat Supply above 150 °C,” Energy Conversion and Management: X, **2**, p. 100011. https://doi.org/10.1016/j.ecmx.2019.100011
[4] Jesper, M., Schlosser, F., Pag, F., Walmsley, T. G., Schmitt, B., and Vajen, K., 2021, “Large-Scale Heat Pumps: Uptake and Performance Modelling of Market-Available Devices,” Renewable and Sustainable Energy Reviews, **137**, p. 110646. https://doi.org/10.1016/j.rser.2020.110646
[5] Naegler, T., Simon, S., Klein, M., and Gils, H. C., 2015, “Quantification of the European Industrial Heat Demand by Branch and Temperature Level: Quantification of European Industrial Heat Demand,” Int. J. Energy Res., 39(15), pp. 2019–2030. https://doi.org/10.1002/er.3436
[6] Rehfeldt, M., Fleiter, T., and Toro, F., 2018, “A Bottom-up Estimation of the Heating and Cooling Demand in European Industry,” Energy Efficiency, 11(5), pp. 1057–1082. https://doi.org/10.1007/s12053-017-9571-y
[7] Thekdi, A., and Nimbalkar, S. U., 2015, *Industrial Waste Heat Recovery - Potential Applications, Available Technologies and Crosscutting R&D Opportunities*, ORNL/TM--2014/622, 1185778.
[8] Gai, L., Varbanov, P. S., Walmsley, T. G., and Klemeš, J. J., 2020, “Critical Analysis of Process Integration Options for Joule-Cycle and Conventional Heat Pumps,” Energies, **13**(3), p. 635. https://doi.org/10.3390/en13030635
[9] Angelino, G., and Invernizzi, C., 1995, “Prospects for Real-Gas Reversed Brayton Cycle Heat Pumps,” International Journal of Refrigeration, **18**(4), pp. 272–280. https://doi.org/10.1016/0140-7007(95)00005-V
[10] 2021, *Thermal, Mechanical, and Hybrid Chemical Energy Storage Systems*, Elsevier.
[11] Oehler, J., Gollasch, J., Tran, A. P., and Nicke, E., 2020, “Part Load Capability of a High Temperature Heat Pump with Reversed Brayton Cycle,” 13th IEA Heat Pump Conference, Jeju, Korea, p. 12.
[12] Oehler, J, Tran, AP, & Stathopoulos, P. "Simulation of a Safe Start-Up Maneuver for a Brayton Heat Pump." *Proceedings of the ASME Turbo Expo 2022: Turbomachinery Technical Conference and Exposition*. *Volume 4: Cycle Innovations; Cycle Innovations: Energy Storage*. Rotterdam, Netherlands. June 13–17, 2022. V004T06A003. ASME. https://doi.org/10.1115/GT2022-79399
[13] Längauer, A., Adler, B., and Rakusch, C., 2020, “Test Results of a Rotation Heat Pump and Further Developments.” 13th IEA Heat Pump Conference, Jeju, Korea
[14] https://www.maltainc.com/. (last accessed 15-05-2023)
[15] https://www.echogen.com/. (last accessed 15-05-2023)
[16] Frate, GF, Pettinari, M, Di Pino Incognito, E, Costanzi, R, & Ferrari, L. "Dynamic Modelling of a Brayton PTES System." *Proceedings of the ASME Turbo Expo 2022: Turbomachinery Technical Conference and Exposition*. *Volume 4: Cycle Innovations; Cycle Innovations: Energy Storage*. Rotterdam, Netherlands. June 13–17, 2022. V004T07A013. ASME. https://doi.org/10.1115/GT2022-83445
[17] Smith, NR, Tom, B, Rimpel, A, Just, J, Marshall, M, Khawly, G, Revak, T, & Hoopes, K. "The Design of a Small-Scale Pumped Heat Energy Storage System for the Demonstration of Controls and Operability." *Proceedings of the ASME Turbo Expo 2022: Turbomachinery Technical Conference and Exposition*. *Volume 4: Cycle Innovations; Cycle Innovations: Energy Storage*. Rotterdam, Netherlands. June 13–17, 2022. V004T07A012. ASME. https://doi.org/10.1115/GT2022-83424
[18] The MathWorks Inc., 2022, “MATLAB Version: 9.13.0 (R2022b).”
[19] Lemmon, E. W., Bell, I. H., Huber, M. L., and McLinden, M. O., 2018, “NIST Standard Reference Database 23: Reference Fluid Thermodynamic and Transport Properties-REFPROP, Version 10.0, National Institute of Standards and Technology.”
[20] Holman, J. P., 2002, *Heat Transfer*, McGraw-Hill, New York, NY.